

This is an Open Access document downloaded from ORCA, Cardiff University's institutional repository: <https://orca.cardiff.ac.uk/id/eprint/120326/>

This is the author's version of a work that was submitted to / accepted for publication.

Citation for final published version:

Al-Sabah, Ayesha, Burnell, Stephanie E.A., Simoes, Irina N., Jessop, Zita, Badieli, Nafiseh, Blain, Emma and Whitaker, Iain S. 2019. Structural and mechanical characterization of crosslinked and sterilised nanocellulose-based hydrogels for cartilage tissue engineering. *Carbohydrate Polymers* 212 , pp. 242-251. 10.1016/j.carbpol.2019.02.057

Publishers page: <http://dx.doi.org/10.1016/j.carbpol.2019.02.057>

Please note:

Changes made as a result of publishing processes such as copy-editing, formatting and page numbers may not be reflected in this version. For the definitive version of this publication, please refer to the published source. You are advised to consult the publisher's version if you wish to cite this paper.

This version is being made available in accordance with publisher policies. See <http://orca.cf.ac.uk/policies.html> for usage policies. Copyright and moral rights for publications made available in ORCA are retained by the copyright holders.



1 **Structural and Mechanical Characterization of Crosslinked and Sterilised Nanocellulose-Based**
2 **Hydrogels for Cartilage Tissue Engineering**

3

4 †Ayesha Al-Sabah^a, †Stephanie EA Burnell^a, †Irina N Simoes^a, Zita Jessop^{a,b}, Nafiseh Badiei^c, Emma
5 Blain^d and *Iain S Whitaker^{a,b}

6 ^aReconstructive Surgery & Regenerative Medicine Group (ReconRegen), Institute of Life Sciences,
7 Swansea University Medical School, SA2 8PP, Swansea, Wales, UK, ^bThe Welsh Centre for Burns
8 and Plastic Surgery, Morriston Hospital, SA6 6NL, Swansea, Wales, UK, ^cNanoHealth Centre,

9 Institute of Life Sciences, Swansea University Medical School, SA2 8QA, Swansea, Wales, UK,

10 ^dArthritis Research UK Biomechanics and Bioengineering Centre, School of Biosciences, Cardiff
11 University, CF10, 3AX, Cardiff, Wales, UK

12 Ayesha Al-Sabah: aishaalsabah@yahoo.com, Stephanie EA Burnell: stephb90@hotmail.co.uk, Irina

13 N Simoes: irina.nevessimoes@swansea.ac.uk, Zita Jessop: z.m.jessop@swansea.ac.uk, Nafiseh

14 Badiei: n.badiei@swansea.ac.uk, Emma Blain: blain@cardiff.ac.uk and Iain S Whitaker:

15 iainwhitaker@fastmail.fm.

16

17 †Equivalent contributors

18

19 **Corresponding author:**

20 Professor Iain S. Whitaker

21 Reconstructive Surgery & Regenerative Medicine Group (ReconRegen)

22 Institute of Life Sciences 2, Swansea University Medical School

23 Swansea, SA2 8PP, Wales, United Kingdom

24 Telephone: +44 1792 606311

25 Fax: +44 1792 703875

26 E-mail: iainwhitaker@fastmail.fm

27 **Abstract**

28 Nanocellulose is a natural biopolymer derived from cellulose. Combined with sodium alginate, it is
29 used to 3D print hydrogels for articular and nasal cartilage engineering and shows good integration,
30 promising cartilage regeneration and mechanical stability over 60 days of implantation in mice. Yet,
31 little is known about their structural and mechanical properties, particularly the impact of crosslinking
32 and sterilisation methods. This study investigates the impact of different calcium chloride crosslinker
33 concentrations and sterilization methods on the structural and mechanical properties of nanocellulose-
34 based hydrogels containing plant-derived cellulose nanofibrils, cellulose nanocrystals or a blend of
35 the two. Crosslinking significantly alters the overall network distribution, surface morphology, pore
36 size and porosity of the hydrogels. Sterilisation has a striking effect on pore size and affects swelling
37 depending on the sterilisation method. The effect of crosslinker and sterilisation on the overall
38 properties of the hydrogels was reliant on the form of nanocellulose that comprised them.

39

40 **Keywords:** Nanocellulose, Crosslinking, Sterilisation, Hydrogels, Cartilage Tissue Engineering

41

42 **1. Introduction**

43 Tissue engineering can provide advanced alternatives to the current standard surgical procedures used
44 in the field of cartilage repair and reconstruction. For many years, the cartilage tissue engineering
45 field has explored the use of biomaterials, more specifically hydrogels, to create tissue substitutes
46 (Park & Lee, 2014; Tibbitt & Anseth, 2009; Xiao, Friis, Gehrke, & Detamore, 2013). Hydrogels
47 mimic the native extracellular matrix (ECM) and can be tailored to resemble the native structure and
48 mechanics of the tissues, enhance mass transport and support cell adhesion and protein sequestration
49 (S. Lin, Sangaj, Razafiarison, Zhang, & Varghese, 2011; Tibbitt & Anseth, 2009). Importantly,
50 through techniques such as three-dimensional (3D) bioprinting, these hydrogels can be used as
51 bioinks to create high-resolution 3D structures, with any shape or size, to support cell growth and
52 tissue formation (Mouser *et al.*, 2017). As the use of synthetic materials often leads to infection,

53 extrusion and foreign body reaction, more natural biomaterials are increasingly explored (Anderson,
54 Rodriguez, & Chang, 2008; Baker, Walsh, Schwartz, & Boyan, 2012).

55 Alginate is a natural and abundant polysaccharide that occurs in marine brown algae and other sources
56 (Hecht & Srebnik, 2016). Water-soluble sodium alginate ((NaC₆H₇O₆)_n), the sodium salt of alginic
57 acid, is commonly used as a component of hydrogels for cartilage engineering due to its recognized
58 chondrogenicity and ability to enhance the structural properties of hydrogels (Ansari *et al.*, 2017;
59 Chou, Akintoye, & Nicoll, 2009; Markstedt *et al.*, 2015; Miao *et al.*, 2017).

60 Within the past decade, nanocellulose (NC) was appointed as an exciting novel biomaterial for
61 biomedical applications due to its attractive physicochemical properties, abundance, sustainability,
62 non-cytotoxicity and biodegradability (Dumanli, 2016; N. Lin & Dufresne, 2014). NC is a biopolymer
63 derived from cellulose, a polysaccharide composed by D-glucopyranose linked by β-1,4 glycosidic
64 bonds (Endes *et al.*, 2016) that is the most abundant, renewable and natural resource available
65 (Dumanli, 2016; N. Lin & Dufresne, 2014). Cellulose contains three hydroxyl groups (-OH) at C-2,
66 C-3 and C-6 positions which determine its physical properties. NC can be found in plants and marine
67 animals and is naturally available in two forms: nanofibrils and nanocrystals (N. Lin & Dufresne,
68 2014). Additionally, NC is biotechnologically produced in bacteria (N. Lin & Dufresne, 2014).

69 Although the cellulose molecular backbone is common to all forms of NC, the surface morphology,
70 size, chemical and physical properties can vary depending on the material source and extraction
71 methods (Mao *et al.*, 2017). Cellulose nanofibrils and nanocrystals are produced through several
72 chemical, mechanical and/or enzymatic methods that introduce functional groups in the surface of
73 the NC (Kim & Song, 2015). Yet, NC produced through the American Value Added Pulping
74 (AVAP[®]) technology chemically pre-treats wood-pulp derived biomass and produces NC that is free
75 from any additional functional groups, apart from the -OH groups (Kyle *et al.*, 2018). Importantly,
76 the lack of post-hydrolysis modifications allows facile surface functionalization of the hydroxyl
77 groups resulting in promising potential for novel, advanced and multifunctional biomaterials with
78 improved biocompatibility and tissue generation (Bodin *et al.*, 2007). Bacterial NC can be produced

79 with high purity and has shown promise for tissue engineering applications (water-holding capacity,
80 mechanical strength and morphological similarities with collagen) and 3D bioprinting (good
81 rheological properties) (Ahrem *et al.*, 2014; Markstedt *et al.*, 2015; Paakko *et al.*, 2007). Yet, the use
82 of bacterial NC for large scale commercialization is limited by the high cost of substrates, low
83 productivity of strains and expensive culture media (Paakko *et al.*, 2007; Revin, Liyaskina,
84 Nazarkina, Bogatyreva, & Shchankin, 2018). Despite the efforts to increase productivity and decrease
85 costs using various waste-products, the production of bacterial NC is still far from large-scale
86 commercialisation and needs further development (Revin *et al.*, 2018). Additionally, there are still
87 concerns regarding residual bacterial toxins/epitopes in bacterial NC (Paakko *et al.*, 2007).

88 The combination of crosslinked sodium alginate and NC has been recently explored for cartilage
89 tissue engineering, for articular and nasal reconstruction (Ahrem *et al.*, 2014; Martínez Ávila *et al.*,
90 2015; Möller *et al.*, 2017; Müller, Öztürk, Arlov, Gatenholm, & Zenobi-Wong, 2016; Nguyen *et al.*,
91 2017). The chondrogenic potential and biocompatibility of these composite hydrogels was reported
92 in both *in vitro* and *in vivo* studies using bacterial NC (Ahrem *et al.*, 2014; Martínez Ávila *et al.*,
93 2015; Möller *et al.*, 2017; Müller *et al.*, 2016; Nguyen *et al.*, 2017; Svensson *et al.*, 2005). Recently,
94 Müller and colleagues used 3D bioprinted alginate-NC hydrogels and articular bovine chondrocytes
95 to demonstrate high cell viability, proliferation and high collagen type II deposition after 28 days in
96 culture (Müller *et al.*, 2016). Similarly, Nguyen *et al.* reported, using the same composite hydrogels
97 as a scaffold for the differentiation of human induced pluripotent stem (iPS) cells, significant increase
98 in RNA expression of chondrogenic markers and matrix deposition. This increase was confirmed by
99 histology staining and immunohistochemistry upon 5 weeks of differentiation (Nguyen *et al.*, 2017).

100 In 2015, Martínez-Avila and his team reported *in vivo* neocartilage formation using co-cultures of
101 human nasoseptal chondrocytes and bone marrow mononuclear cells in bilayer alginate-NC
102 hydrogels (Martínez Ávila *et al.*, 2015). Briefly, the constructs were implanted subcutaneously in
103 nude mice showing non-pathological foreign body reaction, deposition of proteoglycans and collagen

104 type II and increased instantaneous modulus upon 8 weeks of implantation (Martínez Ávila *et al.*,
105 2015).

106 In these composite hydrogels, sodium alginate provides structural integrity through chemical
107 crosslinking promoting the transition of the hydrogel into a solid material (Caliari & Burdick, 2016).
108 Sodium alginate can be ionically crosslinked by adding calcium ions (crosslinker) which substitute
109 the sodium ions in the alginate, creating strong bonds between alginate chains and ultimately creating
110 a mesh (Hecht & Srebnik, 2016). The concentration of crosslinker can regulate the characteristics of
111 the solid material by tailoring its structural and mechanical properties (S. Lin *et al.*, 2011). Such
112 changes affect the network mesh distribution and pore size that ultimately impact cellular phenotype,
113 proliferation and ECM production (Bryant, Chowdhury, Lee, Bader, & Anseth, 2004; Hwang *et al.*,
114 2007; Lien, Ko, & Huang, 2009; Villanueva, Klement, von Deutsch, & Bryant, 2009). In cartilage
115 engineering, this has a particularly significant impact on mass transport and the spatial distribution of
116 the ECM – increased hydrogel mesh size leads to higher collagen content, for example (Bryant &
117 Anseth, 2002; Buxton *et al.*, 2007; Chung, Mesa, Randolph, Yaremchuk, & Burdick, 2006; S. Lin *et al.*,
118 2011). Apart from the extensive body of literature reporting on the chondrogenicity of hydrogels
119 combining sodium alginate and NC, the detailed microenvironment and mechanical properties of
120 these hydrogels remains fairly unknown (Leppiniemi *et al.*, 2017; Markstedt *et al.*, 2015; Martínez
121 Ávila *et al.*, 2015; Müller *et al.*, 2016; Nguyen *et al.*, 2017). Moreover, prior to any application, these
122 hydrogels require sterilisation to limit or prevent the risk of contamination, infection and rejection
123 (Matthews, Gibson, & Samuel, 1994; Veerachamy, Yarlagadda, Manivasagam, & Yarlagadda, 2014).
124 Despite the importance of this topic, less than 1% of the scientific publications in the past decade
125 have focused on the sterilisation methods of hydrogel-based biomedical systems (Galante, Pinto,
126 Colaco, & Serro, 2017). Along with this trend, the effect of sterilisation on the intrinsic properties of
127 NC-based hydrogels also remains elusive. Few studies have performed side-by-side comparison of
128 the architecture, structure and mechanics of the different forms of NC-based hydrogels. Plant-derived

129 cellulose nanofibrils, cellulose nanocrystals and blend, produced using AVAP[®] technology have been
130 thoroughly characterised without additives or crosslinking by Kyle *et al.* in 2018 (Kyle *et al.*, 2018).
131 The first aim was to investigate the effect of crosslinking – using calcium chloride (CaCl₂) – on the
132 structural and mechanical properties of AVAP[®] produced plant-derived cellulose nanofibrils,
133 cellulose nanocrystals and blend (combination of nanofibrils and nanocrystals) NC-based hydrogels
134 combined with sodium alginate. Inspired by the hydrogels described in the literature, NC-based
135 hydrogels were crosslinked using increasing concentrations of crosslinker to understand its impact
136 on the overall architecture and characteristic properties (Ahrem *et al.*, 2014; Martínez Ávila *et al.*,
137 2015; Möller *et al.*, 2017; Müller *et al.*, 2016; Nguyen *et al.*, 2017; Svensson *et al.*, 2005). Secondly,
138 the same type of characterisation was performed upon exposure of the NC-based hydrogels to
139 different sterilisation methods: exposure to ultraviolet (UV) light, autoclaving and ethanol immersion.
140 Finally, the characteristics of the microenvironment of NC-based hydrogels used herein was
141 compared with the reported “ideal” conventional environment for cartilage engineering (Nava,
142 Draghi, Giordano, & Pietrabissa, 2016; Oh, Kim, Im, & Lee, 2010; Pan *et al.*, 2015).

143

144 **2. Hypothesis**

145 The concentration of crosslinker and the sterilisation methods affect the structural and mechanical
146 properties (i.e. pore size, overall network organisation, swelling, porosity and elastic modulus) of
147 NC-based hydrogels.

148

149 **3. Material and Methods**

150 All reagents were purchased from Sigma-Aldrich[®] (Dorset, UK) unless stated otherwise. All reagents
151 were of analytical grade or above.

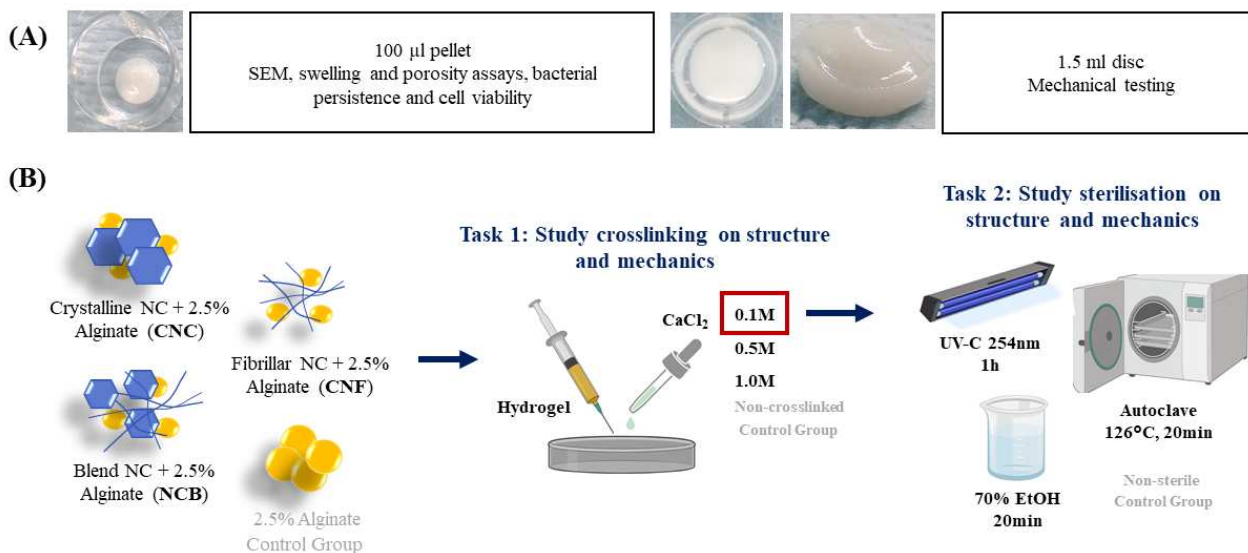
152 **3.1 Preparation of nanocellulose-based hydrogels**

153 Plant-derived nanocellulose (hydrophilic Bioplus[®] cellulose nanofibrils gel, hydrophilic Bioplus[®]
154 cellulose nanocrystals gel and hydrophilic Bioplus[®] blend gel – a blend of fibrils and crystal) was

155 provided by American Process, Inc. (Georgia, USA) (Kyle *et al.*, 2018). All nanocellulose forms are
156 produced via the AVAP® technology (Kyle *et al.*, 2018) which fractionates biomass into cellulose,
157 hemicelluloses and lignin using ethanol and sulfur dioxide (Kyle *et al.*, 2018). The final nanocellulose
158 product morphology – fibrils (3 wt.% solids), crystals (6 wt.% solids) and blend (3 wt.% solids) was
159 controlled by the time and temperature of the pre-treatment step (Kyle *et al.*, 2018). The blend
160 nanocellulose is produced *in situ* during production and is not an actual blend of fibrils and crystal,
161 yet for simplicity it will be referred to as blend. Hydrogels were prepared by mixing nanocellulose
162 with 2.5% (w/v) sodium alginate (alginic acid sodium salt, from brown algae, 80,000-120,000 Da,
163 medium viscosity (2% at 25°C), 1.56 mannuronate/guluronate ratio) solution in ultrapure water.
164 Briefly, nanocellulose was centrifuged at 1500 g for 5 min, excess water was removed, and 2.5%
165 sodium alginate solution was added in a 1:4 proportion (Markstedt *et al.*, 2015). NC-based hydrogels
166 were named as follows: NC-blend and 2.5% sodium alginate (NCB), NC-fibrils and 2.5% sodium
167 alginate (CNF) and NC-crystals and 2.5% sodium alginate (CNC). All NC-based hydrogels contained
168 75% of NC, where CNF and NCB had a final concentration of 2.25 wt.% solids and CNC contained
169 4.5 wt.% solids.

170 **3.2 Crosslinking of nanocellulose-based hydrogels**

171 Nanocellulose-based hydrogels were shaped into: (a) 1.5 ml discs ($\varnothing \approx 14$ mm) for mechanical testing
172 and (b) 100 μ l pellets for all other assays (Figure 1A). The discs were produced using 24 well plates
173 (Cellstar®) and the pellets were produced using 1ml syringes (BD Biosciences®, Oxford, UK) and
174 the indentations of a 96 well plate lid (Cellstar®) as a mould. Crosslinking was performed at room
175 temperature using 0.1 M, 0.5 M or 1.0 M calcium chloride (CaCl₂) solutions prepared in ultrapure
176 water. Hydrogels of 2.5% sodium alginate were also prepared as mentioned above. The experimental
177 layout is depicted in Figure 1B.



178

179 **Figure 1.** Graphical experimental layout. (A) Overall aspect of NC-based hydrogels (pellets and discs). Photos are from
 180 NCB-based crosslinked hydrogels. (B) Experimental layout: different NC-based hydrogels were crosslinked with varying
 181 concentrations of CaCl₂ – structural and mechanical properties were assessed post-crosslinking; NC-based hydrogels
 182 crosslinked with the least concentrated CaCl₂ solution were subjected to different sterilisation methods – structural and
 183 mechanical properties were assessed post-sterilisation. Sodium alginate hydrogels were used as controls in all
 184 experiments. NCB – nanocellulose blend of fibrils and crystal; CNC – nanocellulose crystal; CNF – nanocellulose fibrils;
 185 CaCl₂ – calcium chloride. Image partially created with BioRender©.

186 3.3 Sterilization of nanocellulose-based hydrogels

187 Nanocellulose-based hydrogels were sterilised using (a) autoclave, (b) UV light (UV-C germicidal
 188 light) or (c) ethanol (70% absolute ethanol in ultrapure water). Autoclave sterilisation was performed
 189 for 20 min at 126°C using a Classic bench-size autoclave (Prestige Medical, Blackburn, UK). UV
 190 sterilisation was completed in petri dishes inside a laminar flow hood using UV-C 254 nm for 1 hour.
 191 After sterilisation, hydrogels were crosslinked using 0.1 M CaCl₂. Ethanol sterilisation was carried
 192 out by immersion of nanocellulose-based hydrogels in ethanol for 20 min – the crosslinking was
 193 performed in tandem (*i.e.* the CaCl₂ was dissolved in 70% ethanol). Sodium alginate hydrogels were
 194 also processed as mentioned above. The experimental layout is depicted in Figure 1B.

195 3.4 Scanning electron microscopy and average pore size calculation

196 Hydrogels were washed with 50 mM sodium cacodylate-HCl buffer solution (pH 7.2-7.4, SPI
 197 Supplies®, West Chester, PA, USA) for 10-20 min, fixed overnight in 2% glutaraldehyde and

198 dehydrated using a series of graded ethanol concentrations (30%-100%). These were subsequently
199 rinsed with 50% hexamethyldisilazane solution (HMDS) in 100% ethanol for 10 min, then in 100%
200 HMDS and left overnight to dry. The specimens were coated with a thin layer of gold (~15 nm) using
201 sputter coating and examined using scanning electron microscopy (SEM, Hitachi 4800, Hitachi,
202 Schamamburg, IL, USA). Pore size was determined using ImageJ 1.51 software from the National
203 Institutes of Health, USA.

204 **3.5 Swelling and porosity assays**

205 Pellets were immersed in 1x PBS (Gibco®, ThermoFisher Scientific, Loughborough, UK) and
206 incubated at 37°C for 24 hours. After blotting the excess PBS on the surface, each pellet was weighed
207 individually (M_w). After drying for 48h at room temperature (using desiccant inside a Styrofoam box),
208 the pellets were again weighed individually (M_d). Swelling and porosity percentages (%) were given
209 by the Equation 1 and 2 (Caliari & Burdick, 2016; Gupta & Shivakumar, 2012; K. Pal, 2009). PBS
210 density was considered as 1.06 g cm⁻³.

$$211 \text{ Swelling \%} = \frac{M_w - M_d}{M_d} \times 100 \quad \text{Equation 1}$$

$$212 \text{ Porosity \%} = \frac{(M_w - M_d)}{\rho_{PBS} \times V_{pellet}} \times 100 \quad \text{Equation 2}$$

213 **3.6 Mechanical testing**

214 Mechanical tests were performed on wet discs at room temperature using a Bose Electroforce® 3200
215 (Bose Corp., TA Instruments, MN, USA) equipped with a compression plate. Compressive loading
216 was applied using a 1 Hz frequency at 5 N for 20 cycles. Young's modulus was given by Equation 3,
217 4, and 5.

$$218 \text{ Young's Modulus (kPa)} = \frac{\text{Stress (N m}^{-2}\text{)}}{\text{Strain (\%)}} \quad \text{Equation 3}$$

219 Where,

$$220 \text{ Stress} = \frac{\text{Force (N)}}{\text{Area (m}^2\text{)}} \quad \text{Equation 4}$$

$$221 \text{ Strain} = \frac{\text{Length}_{\text{pre-load}} \text{ (m)} - \text{Length}_{\text{post-load}} \text{ (m)}}{\text{Length}_{\text{pre-load}} \text{ (m)}} \quad \text{Equation 5}$$

222 The length and surface area were determined pre- and post-loading using a digital calliper.

223 **3.7 Bacterial persistence**

224 Bacterial persistence post-sterilisation was determined through optical density (OD) at 600 nm using
225 a spectrophotometer. Samples were horizontally and vertically cut into four equal pieces with similar
226 exposed surface area and added to a tube containing 10 ml of lysogeny broth (LB). After 24h and 48h
227 at 37°C under constant stirring, 1ml samples were taken out and used to measure OD.

228 **3.8 Cell viability**

229 Human naso-septal chondrocytes were isolated from healthy donors, after informed consent from
230 patients (IRAS ID 99202) at ABM University Health Board, Swansea, United Kingdom. Samples
231 were collected during routine septorhinoplasty procedures where the cartilage would have otherwise
232 been discarded (institutional review committee approved the study, ethics approval: REC
233 12/WA/0029), following an adjusted protocol (Dowthwaite *et al.*, 2004; Fickert, Fiedler, & Brenner,
234 2004). Cells were extracted overnight using 2.0 mg ml⁻¹ pronase and 2.4 mg ml⁻¹ collagenase I and
235 cultured in DMEM with 10% fetal bovine serum (FBS), 1% penicillin-streptomycin solution, 1mM
236 D-glucose solution and 0.1% minimum essential medium (MEM) non-essential amino acids (all from
237 Gibco®) in a humidified 37°C incubator with 5% CO₂. After 2.5 weeks, chondrocytes were mixed
238 with the sterilised hydrogels (3 x 10⁵ cells per pellet) to prepare 100 µl pellets, as mentioned
239 previously, and crosslinked using 0.1 M CaCl₂. Pellets were cultured for up to 7 days – cell viability
240 was determined at 24h and 7 days using Live/Dead assay kit (ThermoFisher Scientific) according to
241 manufacturer's instructions. The pellets were imaged using confocal microscopy (Zeiss 710 confocal
242 microscope, Zeiss, Cambridge, UK) and ZEN software (Zeiss).

243 **3.9 Statistical analysis**

244 Data are expressed as mean ± standard error of the mean (mean ± SEM). All data were checked for
245 normality (Anderson-Darling Test) and equal variance (Levene's Test) to meet the assumptions of
246 ANOVA. An ANOVA followed by a Tukey test for *post-hoc* pairwise comparisons were used.

247 Alternatively, Mann-Whitney U tests were used for data with unequal variance. Statistical analysis
248 was performed using Minitab[®] 18 (Minitab Inc.). A p-value < 0.05 was considered significant.

249

250 **4. Results and Discussion**

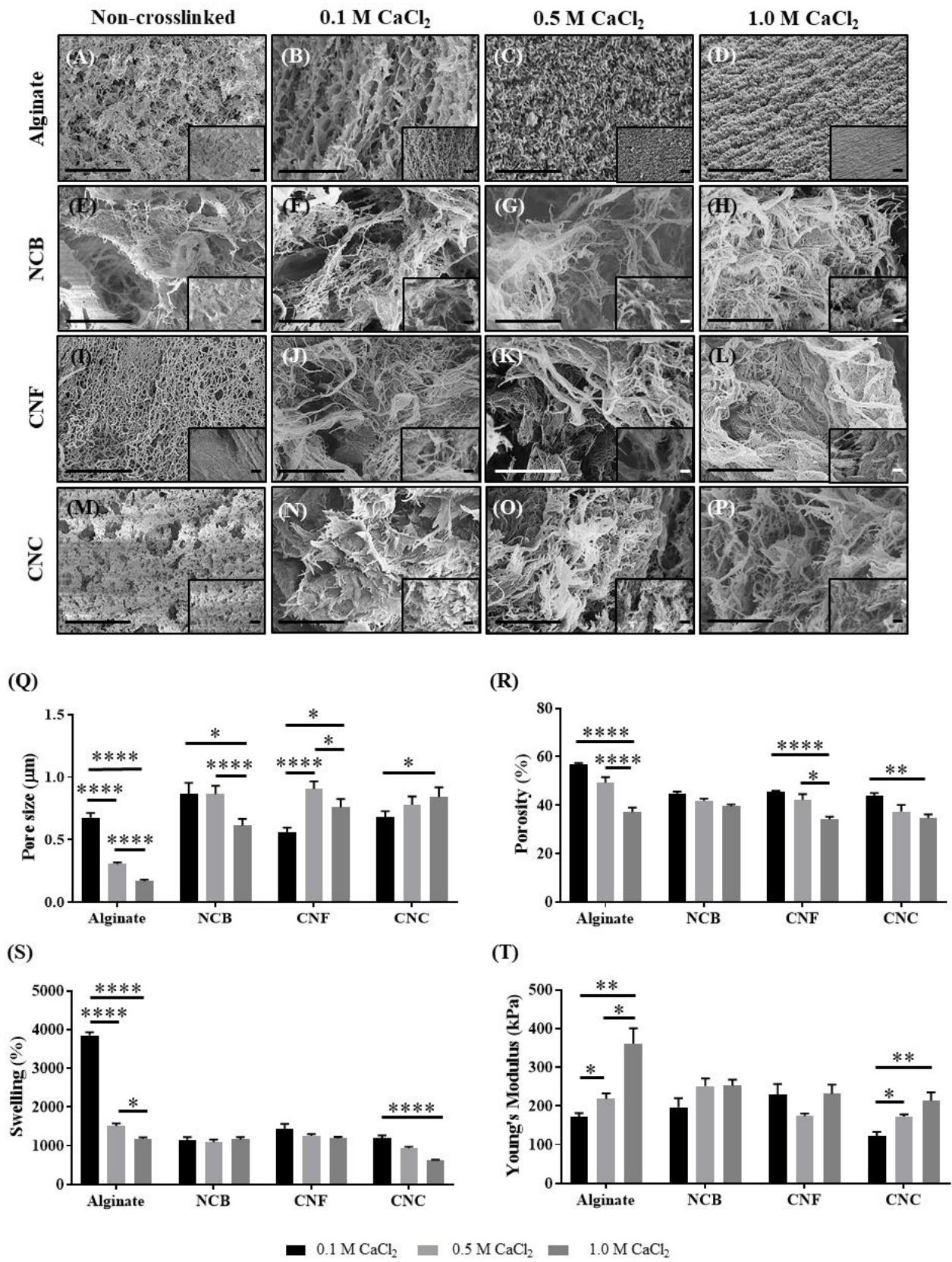
251 In recent years, NC-based hydrogels have been used for cartilage engineering purposes providing
252 promising *in vitro* and *in vivo* outcomes (Martínez Ávila *et al.*, 2015; Nguyen *et al.*, 2017). However,
253 little is known about the effects of crosslinking concentrations and sterilisation methods on the
254 hydrogel structure, microarchitecture, and mechanical properties. If these hydrogels are to be
255 translated to clinic, it is essential to understand how such processing methods affect their properties.
256 In this study, we initially looked at the effect of increasing crosslinker concentrations and later
257 investigated the impact of different sterilisation methods. NC-based hydrogels possess excellent
258 rheological properties for applications such as 3D bioprinting, however these must be supplemented
259 with a biomaterial that enables crosslinking to ensure post-printing shape fidelity (Kyle *et al.*, 2018).
260 To that end, we used plant-derived cellulose nanofibrils, cellulose nanocrystals and a blend, produced
261 via the AVAP[®] technology which do not crosslink on their own when exposed to various
262 concentrations of CaCl₂ (data not shown). Sodium alginate was used to provide structural integrity
263 via ionic crosslinking using CaCl₂ (Hecht & Srebnik, 2016). NC-based hydrogels were formulated
264 by mixing sodium alginate and different NC forms: crystalline (CNC), fibrillar (CNF) and blend
265 (NCB) (Figure 1 and Supplementary Material, Figure S1). The surface charge of the different NC
266 forms were previously evaluated by means of the zeta potential (Kyle *et al.*, 2018). All NC forms
267 showed negative zeta potential in neutral water. As such, this feature was dismissed for the discussion
268 as it would not explain structural and mechanical differences between the composite hydrogels.

269 **4.1 Characterization of crosslinked NC-based hydrogels**

270 The surface morphology and network distribution of the different NC-based hydrogels were observed
271 through SEM images (Figure 2A-P). CNC and CNF showed different surface morphologies – CNF
272 contains a fibrillar-like network with varying thickness (Figure 2I) while CNC holds a leaf-like net

273 architecture (Figure 2M). The overall surface morphology of NCB, a blend of CNC and CNF, is
274 apparently more porous and interconnected than CNF and CNC individually (Figure 2E). Upon
275 addition of the crosslinker, the overall structural morphology and network distribution change
276 noticeably. Increasing concentrations of CaCl₂ developed a denser and more organised network in the
277 sodium alginate hydrogels, creating an apparent flatter external surface (Figure 2A-D). In the NC-
278 based hydrogels the same trend was observed, although visible differences were more obvious when
279 comparing the highest CaCl₂ concentration (Figure 2H, 2L and 2P) with the other two concentrations
280 (Figure 2F-G, 2J-K and 2N-O). As sodium alginate is the structural crosslinked component of the
281 NC-based hydrogels, the NC is in the interstitial framework of sodium alginate and thus seems
282 relatively disorganised, making these changes only noticeable at higher crosslinker concentration.
283 With increasing CaCl₂, the gelation rate increases as it is directly proportional to the concentration of
284 calcium ions (Lee & Rogers, 2012). The resulting hydrogel has increased interactions between
285 sodium alginate chains, as additional binding sites on alginate become occupied by calcium ions
286 (Fang *et al.*, 2007). The network of NC-based hydrogels is moderately different between NCB, CNC
287 and CNF, yet noticeably different from the sodium alginate hydrogels: alginate has a more organised
288 and uniform pore distribution whereas NC-based hydrogels are more irregular with varying pore
289 distribution and pore interconnectivity. These findings are related to the structural organisation of
290 sodium alginate as linear unbranched chains – the differences observed are more prominent due to a
291 higher level of organisation of alginate when compared to NC-based hydrogels (Vold, Kristiansen, &
292 Christensen, 2006). Average pore size was confirmed through ImageJ measurements (Figure 2Q),
293 showing significant differences ($p < 0.05$) in all hydrogels when exposed to the crosslinker. The impact
294 of different CaCl₂ concentrations on pore size was particularly accentuated in the sodium alginate
295 hydrogels ($p < 0.0001$), confirming the tendency observed through SEM (Figure 2A-D). Interestingly,
296 CNC exposed to the lowest CaCl₂ concentration had smaller pores than the ones subjected to the
297 highest concentration ($0.68 \pm 0.05 \mu\text{m}$ versus $0.84 \pm 0.08 \mu\text{m}$, respectively, Figure 2Q). The lower
298 porosity along higher crosslinking concentrations is due to the enhanced association of sodium

299 alginate polymers inadvertently reducing porosity (Peretz *et al.*, 2014) – more crosslinker particles
300 translates into more bonds between the α -L-guluronic chains of sodium alginate (Hecht & Srebnik,
301 2016). CNF showed the same trend as CNC, although a significant decrease ($p < 0.05$) was seen
302 between 0.5M CaCl_2 and 1.0M CaCl_2 (Figure 2Q). Contrarily, the NCB crosslinked with 1.0M CaCl_2
303 showed smaller pore sizes than the ones exposed to lower concentrations ($0.61 \pm 0.05 \mu\text{m}$ versus 0.87
304 $\pm 0.09 \mu\text{m}$ and $0.86 \pm 0.07 \mu\text{m}$, respectively, Figure 2Q). A similar trend was observed when
305 evaluating average pore size at a higher magnification (Supplementary Material, Figure S2A). The
306 differences seen in NC-based hydrogels are possibly due to the diluted sodium alginate polymers tight
307 interaction, but the presence of NC in between the chains prevents the formation of a tighter and
308 organised network as observed with sodium alginate on its own.



309

310 **Figure 2.** Structure and mechanics of NC-based hydrogels post-crosslinking with different CaCl₂ concentrations. (A-P)
 311 Overall network architecture and pore distribution. Images taken at 9k and 20k magnifications. Scale bar = 2 µm. (Q)
 312 Average pore size (µm) post-crosslinking based on 9k magnification SEM images. Mean ± SEM, n=80 measurements.

313 (R) Porosity and (S) swelling percentages post-crosslinking. Mean \pm SEM, n=6. (T) Young's modulus (kPa) based on
314 compression post-crosslinking. Mean \pm SEM, n=6. NCB – nanocellulose blend; CNC – nanocellulose crystal; CNF –
315 nanocellulose fibrils; CaCl₂ – calcium chloride; 0.1M CaCl₂ – black; 0.5M CaCl₂ – light grey; 1.0M CaCl₂ – grey. Mann
316 Whitney (Q and T) and ANOVA (R and S) statistical tests: *, $p \leq 0.05$; **, $p \leq 0.01$; ****, $p \leq 0.0001$.

317

318 The overall porosity of NCB was not affected by the concentration of the crosslinker ($p > 0.05$, Figure
319 2R). In all other hydrogels, the porosity decrease was more accentuated between the lowest and the
320 highest CaCl₂ concentrations: sodium alginate ($56.7 \pm 0.8\%$ versus $37.2 \pm 1.9\%$, $p < 0.0001$), CNF
321 ($45.6 \pm 0.3\%$ versus $34.2 \pm 1.0\%$, $p < 0.0001$) and CNC ($43.7 \pm 1.4\%$ versus $34.6 \pm 1.60\%$, $p < 0.01$)
322 (Figure 2R). The swelling capacity of NCB and CNF was not affected by the crosslinker
323 concentration (Figure 2S). Conversely, the swelling of sodium alginate and CNC was affected by
324 CaCl₂ concentration – swelling decreased to at least half when exposed to 1.0M CaCl₂ ($p < 0.0001$,
325 Figure 2S). Overall, in NC-based hydrogels, the use of 0.5M CaCl₂ showed milder effects for both
326 porosity and swelling percentages (Figures 2R and 2S). Finally, the stiffness of the crosslinked
327 hydrogels was measured based on Young's Modulus (Figure 2T). NCB and CNF retained similar
328 stiffness independent of the crosslinker concentration ($p > 0.05$, Figure 2T). However, CNC and
329 sodium alginate yielded stiffer hydrogels when exposed to higher CaCl₂ concentrations (Figure 2T).
330 These similarities may be related to the ordered structural organisation of both sodium alginate and
331 CNC (Ma *et al.*, 2017). The sodium alginate crosslinked with 1.0M CaCl₂ produced the stiffest
332 hydrogel tested (361 ± 40 kPa, Figure 2T).

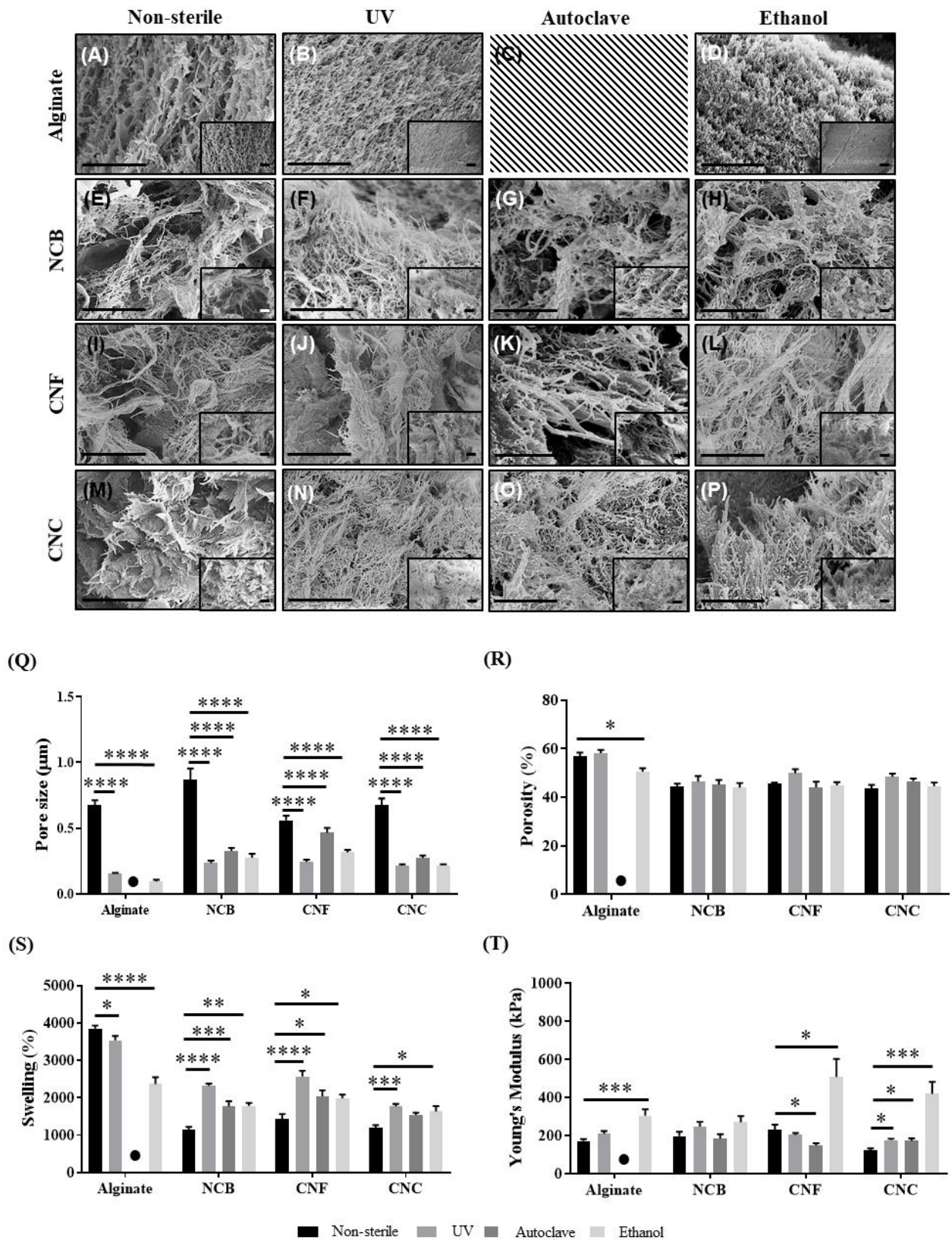
333 Overall, the effect of crosslinker is more striking in sodium alginate hydrogels than NC-based
334 hydrogels. Among the different NC forms, CNC seems to be the most affected by varying crosslinker
335 concentrations while NCB retains most of its characteristics independent of crosslinker
336 concentrations.

337 **4.2 Characterization of sterilised NC-based hydrogels**

338 The use of low crosslinker concentrations has been widely demonstrated as the optimal crosslinking
339 method as it promotes a slower gelation rate, uniform structure, and enhanced mechanical integrity

340 (Kuo & Ma, 2001; Skjåk-Bræk, Grasdalen, & Smidsrød, 1989). As a result, 0.1M CaCl₂ was used to
341 assess the effects of the various sterilisation methods on sodium alginate and NC-based hydrogels.
342 Due to the temperature sensitive nature of sodium alginate, autoclave sterilisation was not pursued as
343 the high temperatures promote depolymerisation of alginate (Leo, McLoughlin, & Malone, 1990).
344 Changes in the surface morphology and network distribution in the different NC-based hydrogels
345 upon sterilisation was confirmed through SEM (Figure 3A-P). All sterilisation methods showed an
346 apparent impact on the overall network distribution. The most striking differences were observed in
347 sodium alginate hydrogels when exposed to any sterilisation method (Figure 3A-D). Both UV and
348 ethanol sterilisations transformed the network of the NC-based hydrogels into a more leaf-like
349 architecture while autoclave seemed to accentuate the fibrillar features of the network (Figure 3E-P).
350 No visible network differences were observed between different NC-based hydrogels exposed to the
351 same sterilisation method. Sterilisation significantly decreased the average pore size of all hydrogels
352 by 17% – 86 % ($p < 0.0001$, Figure 3Q), which is similarly seen in sterilisation of silk-fibroin hydrogels
353 in other studies (Hofmann, Stok, Kohler, Meinel, & Müller, 2014). Autoclave sterilisation resulted in
354 hydrogels with the largest pore size – a trend that was observed in all tested hydrogels (Figure 3Q).
355 Heat sterilisation using the autoclave process replaces the air in the container, creating pressure and
356 leading to the formation of larger pores. Similar trends were observed when evaluating average pore
357 size at a higher magnification (Supplementary Material, Figure S2B). UV and ethanol sterilisations
358 have shown roughly similar pore sizes in all NC-based hydrogels however, the porosity was not
359 affected. This might be related to the rearrangement and fragmentation of the pores during
360 sterilisation, resulting in smaller pores but no changes in overall porosity. This is evident when
361 examining the swelling percentage of NC-based hydrogels. Apart from the alterations in average pore
362 size post-sterilisation, the overall porosity was maintained in all hydrogels except for sodium alginate,
363 where ethanol significantly decreased overall porosity by ~6% ($p < 0.05$, Figure 3R). The swelling
364 capacity of sodium alginate hydrogels decreased significantly post-UV ($p < 0.05$) and post-ethanol
365 sterilisation ($p < 0.0001$, Figure 3S). However, with regards to NC-based hydrogels there was an

366 overall increase in swelling capacity post-sterilisation, with UV sterilisation yielding hydrogels with
367 the highest swelling percentage ($p < 0.001$, Figure 3S). UV irradiation has sufficient energy to disrupt
368 covalent bonds and result in the formation of free radicals which propagate degradation
369 (Wasikiewicz, Yoshii, Nagasawa, Wach, & Mitomo, 2005). The results suggest that UV treatment
370 potentiated the formation of smaller pores which enhanced the swelling potential of all NC-based
371 hydrogels. This is corroborated by the pore size measurements of UV treated NC-based hydrogels.
372 Measurements of stiffness post-sterilisation showed that overall ethanol creates hydrogels with a
373 higher Young's modulus (Figure 3T). This trend was significantly higher in sodium alginate ($306 \pm$
374 32.8 kPa, $p < 0.001$), CNF (508 ± 94.5 kPa, $p < 0.05$), and CNC (420 ± 62.7 kPa, $p < \text{value } 0.001$)
375 hydrogels. Ethanol is known for its dehydration properties resulting in the compaction of hydrogels
376 – which explains the higher mechanical strength post-sterilisation as the resultant gels are stiffer
377 (Eltoum, Fredenburgh, Myers, & Grizzle, 2001). The two other sterilisation methods showed variable
378 effects on hydrogel stiffness (Figure 3T): autoclave sterilisation significantly reduced the Young's
379 modulus of CNF hydrogels (148 ± 12 kPa, $p < 0.05$), whereas it had the opposite effect on CNC
380 hydrogels (173 ± 12.7 kPa, $p < 0.05$). Although it has not been reported in the literature, we theorize
381 that UV and autoclave treatments cause the breakage of clusters of CNC within the hydrogel, resulting
382 in an increase in homogeneity which can be observed in the SEM images post-sterilisation. CNF was
383 not degraded by the thermal energy generated from the autoclave, yet the SEM images show that the
384 fibrils have undergone structural alterations, such as fibril realignment, thus resulting in larger pore
385 size post-sterilisation out of all NC-based hydrogels, which translated into weaker mechanical
386 properties (Kyle *et al.*, 2018; Yang, Yan, Chen, Lee, & Zheng, 2007). All sterilisation methods did
387 not significantly affect the stiffness of NCB hydrogels (Figure 3T). In contrast, all the sterilisation
388 methods used affected the stiffness of CNC (UV, 177 ± 6.6 kPa, $p < 0.05$; autoclave, 173 ± 12.7 kPa,
389 $p < 0.05$; ethanol, 420 ± 62.7 kPa, $p < 0.001$, Figure 3T).



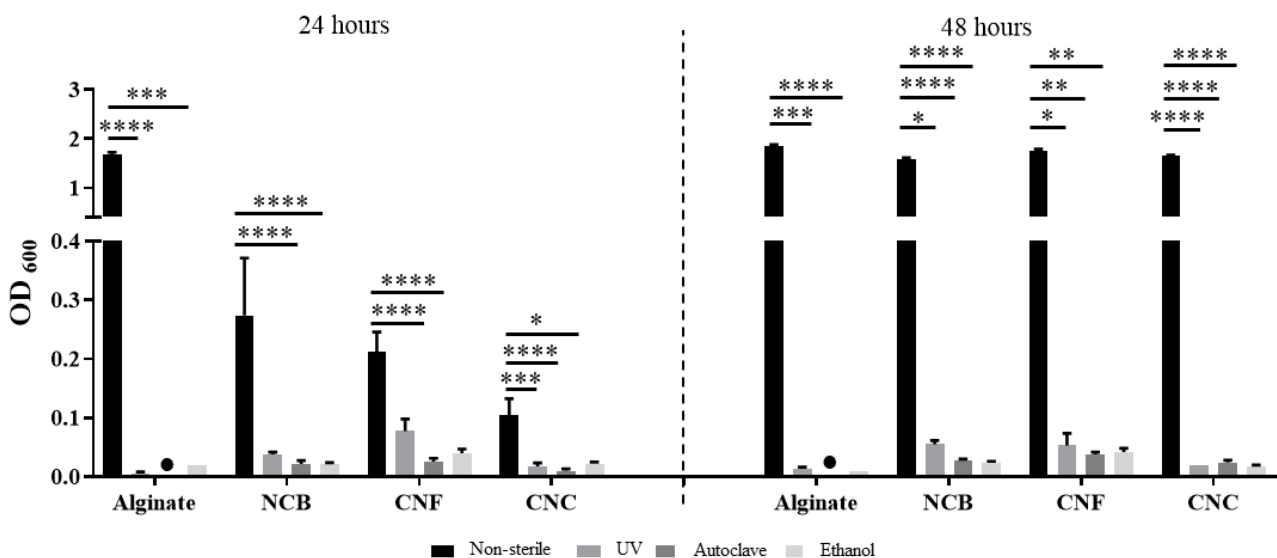
390

391 **Figure 3.** Structure and mechanics of NC-based hydrogels post-sterilisation with different methods. (A-P) Overall
 392 network architecture and pore distribution. Images taken at 9k and 20k magnification. Scale bar = 2 µm. (Q) Average
 393 pore size (µm) post-sterilisation based on 9k magnification SEM images. Mean ± SEM, n=80 measurements. (R) Porosity
 394 and (S) swelling percentages post-sterilisation. Mean ± SEM, n=5-6. (T) Young's modulus (kPa) based on compression

395 post-sterilisation. Mean \pm SEM, n=6. NCB – nanocellulose blend; CNC – nanocellulose crystal; CNF – nanocellulose
 396 fibrils; Non-sterile – black; UV – grey; Autoclave – dark grey; Ethanol – light grey. ●, absent graph bar: autoclaved
 397 sodium alginate hydrogels were not tested. Mann Whitney (Q and T) and ANOVA (R and S) statistical tests: *, $p \leq 0.05$;
 398 **, $p \leq 0.01$; ***, $p \leq 0.001$; ****, $p \leq 0.0001$.

399 4.3 Bacterial persistence in sterilised NC-based hydrogels

400 The efficiency of the sterilisation processes was examined through bacterial persistence (Figure 4).
 401 Sterilisation efficiency was evaluated using the respective non-sterile material as a control and all
 402 sterilisation methods were confirmed as effective in removing bacterial content. All sterilisation
 403 methods showed significant reduction of OD in the hydrogels post-sterilisation ($p < 0.05$, Figure 4).
 404 Overall, UV sterilisation was the most inefficient method for the sterilisation of NC-based hydrogels
 405 (Figure 4). UV sterilisation was very efficient in sodium alginate hydrogels, indicating it is optimal
 406 for materials that are transparent – due to its limited penetrability – but not ideal for NC-based
 407 hydrogels (Lerouge, 2012). Conversely, the autoclave method was the most efficient for all hydrogels
 408 ($p < 0.0001$, Figure 4). Although it resulted in structural alterations, it is the optimal method to ensure
 409 the elimination of potential contaminants including fungal and bacterial spores (Rogers, 2012). In
 410 practice, the use of ethanol is unfeasible as this would result in cell death, as observed in the cell
 411 viability tests.



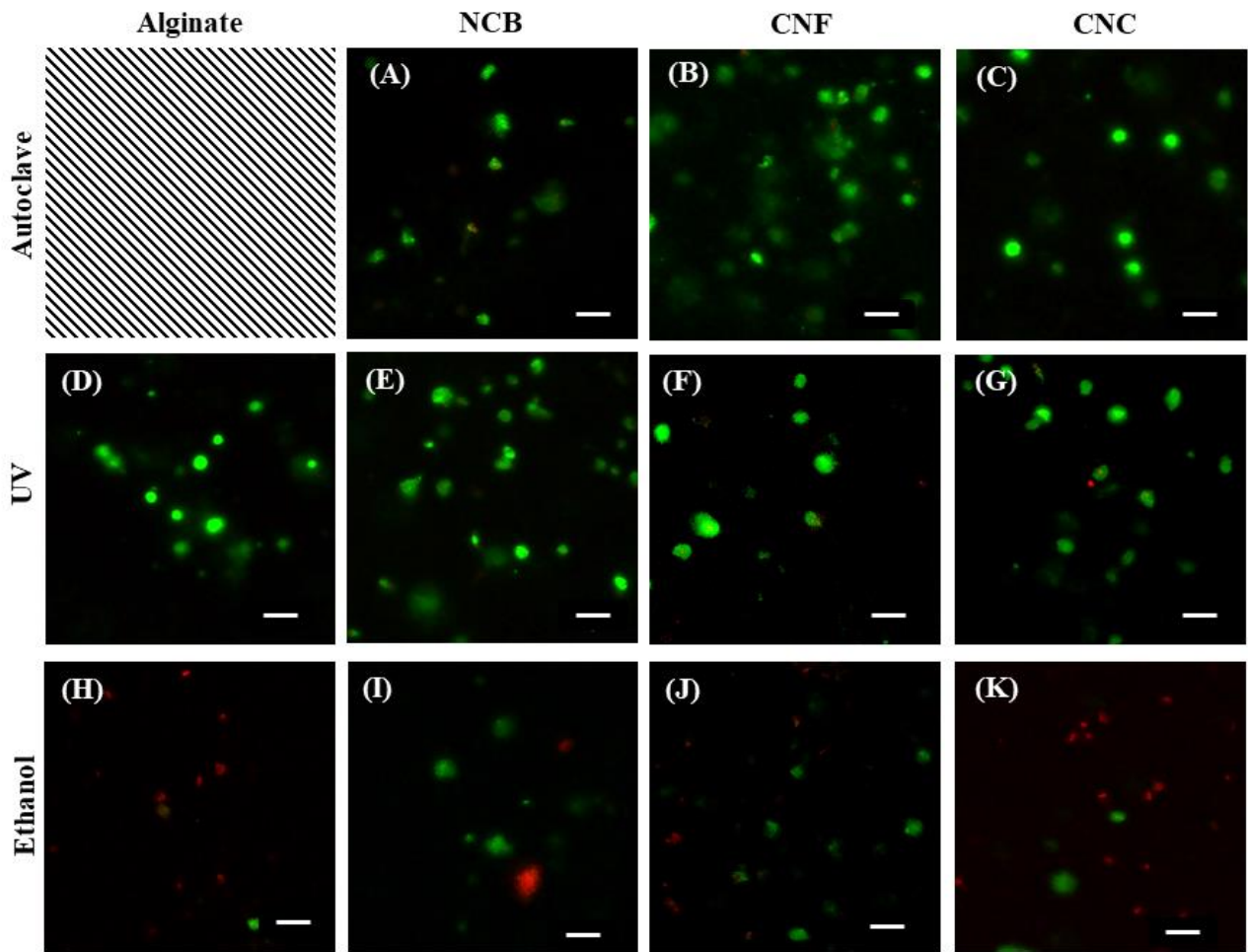
412
 413 **Figure 4.** Bacterial persistence at 24h and 48h post-sterilisation. Mean \pm SEM, n=4-5. NCB – nanocellulose blend; CNC
 414 – nanocellulose crystal; CNF – nanocellulose fibrils. Non-sterile – black; UV – grey; Autoclave – dark grey; Ethanol –

415 light grey. ●, absent graph bar: autoclaved sodium alginate hydrogels were not tested. Mann Whitney statistical test: *, p
416 ≤ 0.05 ; **, $p \leq 0.01$; ***, $p \leq 0.001$; ****, $p \leq 0.0001$.

417 **4.4 Cell viability assessment using sterilised NC-based hydrogels**

418 Cell viability in the hydrogels was assessed at 1- and 7-days post-sterilisation using human naso-
419 septal chondrocytes and Live/Dead[®] assay kit (Figure 5 and Supplementary Material, Figure S3).
420 Upon 24h in culture in sterilised hydrogels, cell viability was minimally affected, apart from the cells
421 in ethanol-sterilised hydrogels where most of the cells were dead (Figure 5). After 7 days, the number
422 of dead cells increased in all hydrogels although it was visibly lower than the number of live cells
423 which is indicative of cellular turnover (Supplementary Material, Figure S3). Yet, the low cell
424 viability outcomes in ethanol sterilisation could be related to a limitation of this study – ethanol
425 sterilisation and crosslinking were performed in tandem, meaning that the cells were exposed to 70%
426 ethanol for 20 min, which resulted in higher cell death when compared to other methods. Technically,
427 for the ethanol sterilisation, it was not possible to sterilise the non-crosslinked NC-based hydrogels
428 with ethanol because the removal of ethanol by centrifugation would result in decreased water content
429 in the hydrogels.

430



431

432 **Figure 5.** Representative cell viability on sterilised hydrogels after 24h under standard culture. Live cells are stained
 433 green and dead cells are stained red as assessed using Live/Dead assay kit®. Crossed out panel represents non-tested
 434 condition – autoclaved sodium alginate hydrogels. Scale bar = 50 μm .

435

436 Importantly, these characterization studies showed that the properties of NC-based hydrogels do not
 437 fall under the “conventional” ideal chondrogenic environment described in the literature – 75-400 μm
 438 pores and 75-97% porosity (Ahrem *et al.*, 2014; Markstedt *et al.*, 2015; Martínez Ávila *et al.*, 2015;
 439 Möller *et al.*, 2017; Müller *et al.*, 2016; Nava *et al.*, 2016; Nguyen *et al.*, 2017; Oh *et al.*, 2010; Pan
 440 *et al.*, 2015). In general, the NC-based hydrogels had 34-50% porosity and with average pore sizes
 441 ranging from 0.22 μm to 0.91 μm , depending on the NC form assessed. This demonstrates that the
 442 definition of ideal environment for cartilage engineering might be broader than expected.

443

444 **5. Conclusion**

445 Previous studies have shown that NC contains favourable properties for diverse biological and
446 medical applications. NC-based hydrogels have been extensively explored for cartilage engineering
447 purposes, mainly using 3D bioprinting technologies.

448 In this study, composite hydrogels containing sodium alginate and different forms of plant-derived
449 NC (nanocellulose fibrils, nanocellulose crystals or a blend), ionically crosslinked with CaCl_2 , were
450 shown to have alterations in their structural and mechanical properties upon standard processing
451 methods such as crosslinking and sterilisation. Increasing concentrations of the crosslinker CaCl_2
452 yielded visible changes in overall architecture, pore size (as demonstrated through SEM) and porosity.
453 As sodium alginate crosslinks faster with increasing concentrations of CaCl_2 , the resulting mesh
454 network will have a different distribution and size, with the different NC forms entrapped in the
455 interstitial areas of the mesh – providing characteristic architectures according their structure (i.e.
456 fibrils or crystals). The swelling capacity and the mechanical properties (as assessed by the Young's
457 Modulus) of the NC-based hydrogels were also affected with increasing crosslinker concentrations,
458 yet not all NC forms were significantly affected.

459 When exposed to different sterilisation methods (physical, thermal and chemical), the crosslinked
460 NC-based hydrogels showed striking significant decreases in average pore size, while porosity was
461 maintained. From all the properties tested, pore size was the most affected by the sterilisation method,
462 possibly due to the re-arrangement of particles inside the hydrogels. The mechanical properties of the
463 hydrogels were mildly affected by the sterilisation method, apart from the chemical sterilisation using
464 ethanol that yielded significantly stronger hydrogels, possibly due to the dehydration of the hydrogels.
465 Importantly, differential effects were observed based on the NC form contained in the composite
466 hydrogels. Among the NC forms, CNC was more affected by the crosslinker concentrations, CNF
467 and CNC were affected by all sterilization methods with different methods affecting properties
468 differently while NCB was more resilient to changes when exposed to different sterilisation methods
469 and crosslinker concentrations. This indicates that the crosslinking reactions and the sterilisation

470 method used to process these hydrogels need to be chosen and tailored to the final aim (e.g. tissue
471 type) as these will significantly alter the final environment to which cells will be exposed.

472 The study of structural and mechanical alterations upon different processing methods is important as
473 it impacts the characteristics of the final product. These will directly affect, for example, its
474 microstructure and microenvironment, ultimately impacting cell phenotype and behaviour when
475 targeting biomedical applications.

476

477 **Acknowledgments**

478 This work was supported by Abertawe Bro Morgannwg University (ABMU) Health Board, Health
479 and Care Research Wales, Oakgrove Medical Charitable Trust, the Royal College of Surgeons of
480 England and the Medical Research Council (grant no. MR/N002431/1). We acknowledge the
481 Arthritis Research UK Biomechanics and Bioengineering Centre (Cardiff University) for access to
482 the ElectroForce™ 3200 loading equipment and Mrs. Kavitha Saw for collecting the human naso-
483 septal samples at Singleton Hospital, Swansea, UK. Dr. Ayesha Al-Sabah, Dr. Stephanie EA Burnell,
484 and Dr. Irina N Simoes have equally contributed to this work.

485

486 **References**

487 Ahrem, H., Pretzel, D., Endres, M., Conrad, D., Courseau, J., Müller, H., . . . Kinne, R. W. (2014). Laser-structured
488 bacterial nanocellulose hydrogels support ingrowth and differentiation of chondrocytes and show potential as cartilage
489 implants. *Acta Biomaterialia*, 10(3), 1341-1353.

490 Anderson, J. M., Rodriguez, A., & Chang, D. T. (2008). Foreign body reaction to biomaterials. *Semin Immunol*, 20(2),
491 86-100.

492 Ansari, S., Diniz, I. M., Chen, C., Aghaloo, T., Wu, B. M., Shi, S., & Moshaverinia, A. (2017). Alginate/hyaluronic
493 acid hydrogel delivery system characteristics regulate the differentiation of periodontal ligament stem cells toward
494 chondrogenic lineage. *J Mater Sci Mater Med*, 28(10), 162.

495 Baker, M. I., Walsh, S. P., Schwartz, Z., & Boyan, B. D. (2012). A review of polyvinyl alcohol and its uses in cartilage
496 and orthopedic applications. *J Biomed Mater Res B Appl Biomater*, 100(5), 1451-1457.

497 Bodin, A., Ahrenstedt, L., Fink, H., Brumer, H., Risberg, B., & Gatenholm, P. (2007). Modification of nanocellulose
498 with a xyloglucan-RGD conjugate enhances adhesion and proliferation of endothelial cells: implications for tissue
499 engineering. *Biomacromolecules*, 8(12), 3697-3704.

- 500 Bryant, S. J., & Anseth, K. S. (2002). Hydrogel properties influence ECM production by chondrocytes
501 photoencapsulated in poly(ethylene glycol) hydrogels. *J Biomed Mater Res*, 59(1), 63-72.
- 502 Bryant, S. J., Chowdhury, T. T., Lee, D. A., Bader, D. L., & Anseth, K. S. (2004). Crosslinking density influences
503 chondrocyte metabolism in dynamically loaded photocrosslinked poly(ethylene glycol) hydrogels. *Ann Biomed Eng*,
504 32(3), 407-417.
- 505 Buxton, A. N., Zhu, J., Marchant, R., West, J. L., Yoo, J. U., & Johnstone, B. (2007). Design and characterization of
506 poly(ethylene glycol) photopolymerizable semi-interpenetrating networks for chondrogenesis of human mesenchymal
507 stem cells. *Tissue Eng*, 13(10), 2549-2560.
- 508 Caliari, S. R., & Burdick, J. A. (2016). A practical guide to hydrogels for cell culture. *Nat Methods*, 13(5), 405-414.
- 509 Chou, A. I., Akintoye, S. O., & Nicoll, S. B. (2009). Photo-crosslinked Alginate Hydrogels Support Enhanced Matrix
510 Accumulation by Nucleus Pulposus Cells In Vivo. *Osteoarthritis and cartilage / OARS, Osteoarthritis Research*
511 *Society*, 17(10), 1377-1384.
- 512 Chung, C., Mesa, J., Randolph, M. A., Yaremchuk, M., & Burdick, J. A. (2006). Influence of gel properties on
513 neocartilage formation by auricular chondrocytes photoencapsulated in hyaluronic acid networks. *J Biomed Mater Res*
514 *A*, 77(3), 518-525.
- 515 Douthwaite, G. P., Bishop, J. C., Redman, S. N., Khan, I. M., Rooney, P., Evans, D. J., . . . Archer, C. W. (2004). The
516 surface of articular cartilage contains a progenitor cell population. *J Cell Sci*, 117(Pt 6), 889-897.
- 517 Dumanli, A. G. (2016). Nanocellulose and its Composites for Biomedical Applications. *Curr Med Chem*.
- 518 Eltoun, I., Fredenburgh, J., Myers, R. B., & Grizzle, W. E. (2001). Introduction to the Theory and Practice of Fixation
519 of Tissues. *Journal of Histotechnology*, 24(3), 173-190.
- 520 Endes, C., Camarero-Espinosa, S., Mueller, S., Foster, E. J., Petri-Fink, A., Rothen-Rutishauser, B., . . . Clift, M. J. D.
521 (2016). A critical review of the current knowledge regarding the biological impact of nanocellulose. *Journal of*
522 *Nanobiotechnology*, 14.
- 523 Fickert, S., Fiedler, J., & Brenner, R. E. (2004). Identification of subpopulations with characteristics of mesenchymal
524 progenitor cells from human osteoarthritic cartilage using triple staining for cell surface markers. *Arthritis Res Ther*,
525 6(5), R422-432.
- 526 Galante, R., Pinto, T. J. A., Colaco, R., & Serro, A. P. (2017). Sterilization of hydrogels for biomedical applications: A
527 review. *J Biomed Mater Res B Appl Biomater*.
- 528 Gupta, N. V., & Shivakumar, H. G. (2012). Investigation of Swelling Behavior and Mechanical Properties of a pH-
529 Sensitive Superporous Hydrogel Composite. *Iran J Pharm Res*, 11(2), 481-493.
- 530 Hecht, H., & Srebnik, S. (2016). Structural Characterization of Sodium Alginate and Calcium Alginate.
531 *Biomacromolecules*, 17(6), 2160-2167.

- 532 Hofmann, S., Stok, K. S., Kohler, T., Meinel, A. J., & Müller, R. (2014). Effect of sterilization on structural and
533 material properties of 3-D silk fibroin scaffolds. *Acta Biomaterialia*, 10(1), 308-317.
- 534 Hwang, N. S., Varghese, S., Lee, H. J., Theprungsirikul, P., Canver, A., Sharma, B., & Elisseeff, J. (2007). Response of
535 zonal chondrocytes to extracellular matrix-hydrogels. *FEBS Lett*, 581(22), 4172-4178.
- 536 K. Pal, A. K. B., D. K. Majumdar. (2009). Polymeric Hydrogels: Characterization and Biomedical Applications - A
537 mini review. *Designed Monomers and Polymers*, 12, 34.
- 538 Kim, D. H., & Song, Y. S. (2015). Rheological behavior of cellulose nanowhisker suspension under magnetic field.
539 *Carbohydr Polym*, 126, 240-247.
- 540 Kuo, C. K., & Ma, P. X. (2001). Ionically crosslinked alginate hydrogels as scaffolds for tissue engineering: Part 1.
541 Structure, gelation rate and mechanical properties. *Biomaterials*, 22(6), 511-521.
- 542 Kyle, S., Jessop, Z. M., Al-Sabah, A., Hawkins, K., Lewis, A., Maffei, T., . . . Whitaker, I. S. (2018). Characterization
543 of pulp derived nanocellulose hydrogels using AVAP(R) technology. *Carbohydr Polym*, 198, 270-280.
- 544 Leo, W. J., McLoughlin, A. J., & Malone, D. M. (1990). Effects of Sterilization Treatments on Some Properties of
545 Alginate Solutions and Gels. *Biotechnology Progress*, 6(1), 51-53.
- 546 Leppiniemi, J., Lahtinen, P., Paajanen, A., Mahlberg, R., Metsa-Kortelainen, S., Pinomaa, T., . . . Hytonen, V. P.
547 (2017). 3D-Printable Bioactivated Nanocellulose-Alginate Hydrogels. *ACS Appl Mater Interfaces*, 9(26), 21959-21970.
- 548 Lerouge, S. (2012). *5 - Non-traditional sterilization techniques for biomaterials and medical devices*. In S. Lerouge &
549 A. Simmons (Eds.), *Sterilisation of Biomaterials and Medical Devices* (pp. 97-116): Woodhead Publishing
- 550 Lien, S. M., Ko, L. Y., & Huang, T. J. (2009). Effect of pore size on ECM secretion and cell growth in gelatin scaffold
551 for articular cartilage tissue engineering. *Acta Biomater*, 5(2), 670-679.
- 552 Lin, N., & Dufresne, A. (2014). Nanocellulose in biomedicine: Current status and future prospect. *European Polymer*
553 *Journal*, 59, 24.
- 554 Lin, S., Sangaj, N., Razafiarison, T., Zhang, C., & Varghese, S. (2011). Influence of physical properties of biomaterials
555 on cellular behavior. *Pharm Res*, 28(6), 1422-1430.
- 556 Ma, X., Li, R., Zhao, X., Ji, Q., Xing, Y., Sunarso, J., & Xia, Y. (2017). Biopolymer composite fibres composed of
557 calcium alginate reinforced with nanocrystalline cellulose. *Composites Part A: Applied Science and Manufacturing*, 96,
558 155-163.
- 559 Mao, Y., Liu, K., Zhan, C., Geng, L., Chu, B., & Hsiao, B. S. (2017). Characterization of Nanocellulose Using Small-
560 Angle Neutron, X-ray, and Dynamic Light Scattering Techniques. *J Phys Chem B*, 121(6), 1340-1351.
- 561 Markstedt, K., Mantas, A., Tournier, I., Martínez Ávila, H., Hägg, D., & Gatenholm, P. (2015). 3D Bioprinting Human
562 Chondrocytes with Nanocellulose–Alginate Bioink for Cartilage Tissue Engineering Applications. *Biomacromolecules*,
563 16(5), 1489-1496.

- 564 Martínez Ávila, H., Feldmann, E.-M., Pleumeekers, M. M., Nimeskern, L., Kuo, W., de Jong, W. C., . . . Gatenholm, P.
565 (2015). Novel bilayer bacterial nanocellulose scaffold supports neocartilage formation in vitro and in vivo.
566 *Biomaterials*, 44, 122-133.
- 567 Matthews, I. P., Gibson, C., & Samuel, A. H. (1994). Sterilisation of implantable devices. *Clin Mater*, 15(3), 191-215.
- 568 Miao, Z., Lu, Z., Wu, H., Liu, H., Li, M., Lei, D., . . . Zhao, J. (2017). Collagen, agarose, alginate and Matrigel
569 hydrogels as cell substrates for culture of chondrocytes in vitro: A comparative study. *J Cell Biochem*.
- 570 Möller, T., Amoroso, M., Hägg, D., Brantsing, C., Rotter, N., Apelgren, P., . . . Gatenholm, P. (2017). In Vivo
571 Chondrogenesis in 3D Bioprinted Human Cell-laden Hydrogel Constructs. *Plastic and Reconstructive Surgery Global
572 Open*, 5(2), e1227.
- 573 Mouser, V. H. M., Levato, R., Bonassar, L. J., D'Lima, D. D., Grande, D. A., Klein, T. J., . . . Malda, J. (2017). Three-
574 Dimensional Bioprinting and Its Potential in the Field of Articular Cartilage Regeneration. *Cartilage*, 8(4), 327-340.
- 575 Müller, M., Öztürk, E., Arlov, Ø., Gatenholm, P., & Zenobi-Wong, M. (2016). Alginate Sulfate–Nanocellulose Bioinks
576 for Cartilage Bioprinting Applications. *Annals of Biomedical Engineering*, 1-14.
- 577 Nava, M. M., Draghi, L., Giordano, C., & Pietrabissa, R. (2016). The effect of scaffold pore size in cartilage tissue
578 engineering. *J Appl Biomater Funct Mater*, 14(3), e223-229.
- 579 Nguyen, D., Hagg, D. A., Forsman, A., Ekholm, J., Nimkingratana, P., Brantsing, C., . . . Simonsson, S. (2017).
580 Cartilage Tissue Engineering by the 3D Bioprinting of iPS Cells in a Nanocellulose/Alginate Bioink. *Sci Rep*, 7(1), 658.
- 581 Oh, S. H., Kim, T. H., Im, G. I., & Lee, J. H. (2010). Investigation of pore size effect on chondrogenic differentiation of
582 adipose stem cells using a pore size gradient scaffold. *Biomacromolecules*, 11(8), 1948-1955.
- 583 Paakko, M., Ankerfors, M., Kosonen, H., Nykanen, A., Ahola, S., Osterberg, M., . . . Lindstrom, T. (2007). Enzymatic
584 hydrolysis combined with mechanical shearing and high-pressure homogenization for nanoscale cellulose fibrils and
585 strong gels. *Biomacromolecules*, 8(6), 1934-1941.
- 586 Pan, Z., Duan, P., Liu, X., Wang, H., Cao, L., He, Y., . . . Ding, J. (2015). Effect of porosities of bilayered porous
587 scaffolds on spontaneous osteochondral repair in cartilage tissue engineering. *Regen Biomater*, 2(1), 9-19.
- 588 Park, H., & Lee, K. Y. (2014). Cartilage regeneration using biodegradable oxidized alginate/hyaluronate hydrogels. *J
589 Biomed Mater Res A*, 102(12), 4519-4525.
- 590 Peretz, S., Florea-Spirou, M., Anghel, D.-F., Bala, D., Stoian, C., & Zgherea, G. (2014). *Preparation of Porous
591 Calcium Alginate Beads and Their Use for Adsorption of O-Nitrophenol from Aqueous Solutions*.
- 592 Revin, V., Liyaskina, E., Nazarkina, M., Bogatyreva, A., & Shchankin, M. (2018). Cost-effective production of
593 bacterial cellulose using acidic food industry by-products. *Braz J Microbiol*, 49 Suppl 1, 151-159.
- 594 Rogers, W. J. (2012). 2 - Steam and dry heat sterilization of biomaterials and medical devices. In S. Lerouge & A.
595 Simmons (Eds.), *Sterilisation of Biomaterials and Medical Devices* (pp. 20-55): Woodhead Publishing

- 596 Skjåk-Bræk, G., Grasdalen, H., & Smidsrød, O. (1989). Inhomogeneous polysaccharide ionic gels. *Carbohydr Polym*,
597 10(1), 31-54.
- 598 Svensson, A., Nicklasson, E., Harrah, T., Panilaitis, B., Kaplan, D. L., Brittberg, M., & Gatenholm, P. (2005). Bacterial
599 cellulose as a potential scaffold for tissue engineering of cartilage. *Biomaterials*, 26(4), 419-431.
- 600 Tibbitt, M. W., & Anseth, K. S. (2009). Hydrogels as extracellular matrix mimics for 3D cell culture. *Biotechnol*
601 *Bioeng*, 103(4), 655-663.
- 602 Veerachamy, S., Yarlagadda, T., Manivasagam, G., & Yarlagadda, P. K. (2014). Bacterial adherence and biofilm
603 formation on medical implants: a review. *Proc Inst Mech Eng H*, 228(10), 1083-1099.
- 604 Villanueva, I., Klement, B. J., von Deutsch, D., & Bryant, S. J. (2009). Cross-linking density alters early metabolic
605 activities in chondrocytes encapsulated in poly(ethylene glycol) hydrogels and cultured in the rotating wall vessel.
606 *Biotechnol Bioeng*, 102(4), 1242-1250.
- 607 Wasikiewicz, J. M., Yoshii, F., Nagasawa, N., Wach, R. A., & Mitomo, H. (2005). Degradation of chitosan and sodium
608 alginate by gamma radiation, sonochemical and ultraviolet methods. *Radiation Physics and Chemistry*, 73(5), 287-295.
- 609 Xiao, Y., Friis, E. A., Gehrke, S. H., & Detamore, M. S. (2013). Mechanical testing of hydrogels in cartilage tissue
610 engineering: beyond the compressive modulus. *Tissue Eng Part B Rev*, 19(5), 403-412.
- 611 Yang, H., Yan, R., Chen, H., Lee, D. H., & Zheng, C. (2007). Characteristics of hemicellulose, cellulose and lignin
612 pyrolysis. *Fuel*, 86(12), 1781-1788.
- 613